

# Industrial Chemistry & Materials

Accepted Manuscript

This article can be cited before page numbers have been issued, to do this please use: S. Cong, S. Sun, Y. Zhang, M. Wang, Z. Jia, J. Peng and H. Pang, *Ind. Chem. Mater.*, 2025, DOI: 10.1039/D5IM00114E.



This is an Accepted Manuscript, which has been through the Royal Society of Chemistry peer review process and has been accepted for publication.

Accepted Manuscripts are published online shortly after acceptance, before technical editing, formatting and proof reading. Using this free service, authors can make their results available to the community, in citable form, before we publish the edited article. We will replace this Accepted Manuscript with the edited and formatted Advance Article as soon as it is available.

You can find more information about Accepted Manuscripts in the [Information for Authors](#).

Please note that technical editing may introduce minor changes to the text and/or graphics, which may alter content. The journal's standard [Terms & Conditions](#) and the [Ethical guidelines](#) still apply. In no event shall the Royal Society of Chemistry be held responsible for any errors or omissions in this Accepted Manuscript or any consequences arising from the use of any information it contains.

## ARTICLE

**Design and construction of homogeneous heterogeneity Co-Zn-ZIF-L membranes for efficient H<sub>2</sub>/CO<sub>2</sub> separation**Received 00th January 20xx,  
Accepted 00th January 20xx

DOI: 10.1039/x0xx00000x

Shenzhen Cong,<sup>†a</sup> Si Sun,<sup>†a</sup> Yijing Zhang,<sup>a</sup> Ming Wang,<sup>a</sup> Zhehua Jia<sup>a</sup>, Jiaoyu Peng<sup>\*b</sup> and Huan Pang<sup>\*a</sup>

Metal-organic framework (MOF) membranes have been extensively researched as an innovative membrane material for H<sub>2</sub>/CO<sub>2</sub> separation. The preparation of MOF membranes can be extended by constructing MOF membranes with homogeneous heterogeneous structure and the MOF membranes with high permeance and high selectivity can be prepared. Here, we use the chelation-assisted interfacial growth process to construct a seeding layer, and then prepare Co-Zn-ZIF-L membranes with homogeneous heterogeneous structure by secondary growth for the efficient separation of H<sub>2</sub>/CO<sub>2</sub>. The resulting Co-Zn-ZIF-L membranes show an H<sub>2</sub> permeances of 2156 GPU and the H<sub>2</sub>/CO<sub>2</sub> selectivity of 31.6 at 298K and 1.0 bar, surpassing the Robeson upper bound (2008). Furthermore, the Co-Zn-ZIF-L membrane has a H<sub>2</sub>/CO<sub>2</sub> separation stability of 65 h and can efficiently separate to obtain pure H<sub>2</sub>.

Keywords: ZIF-L membrane; Oriented growth; H<sub>2</sub>/CO<sub>2</sub> separation; Gas separation.

**1. Introduction**

Hydrogen (H<sub>2</sub>) is an important industrial gas and has already occupied a significant position in industries.<sup>1</sup> Currently, H<sub>2</sub> in industry is primarily derived from the water-gas shift process of fossil fuels. However, the water-gas shift process produces a substantial amount of CO<sub>2</sub>, low concentration of CO, trace H<sub>2</sub>S, and so forth, which is insufficient to meet industrial requirements.<sup>2</sup> H<sub>2</sub> purification typically necessitates a significant investment in the separation process as well as running expenditures, raising the price of hydrogen significantly. Therefore, it is vital to explore an efficient and low-cost H<sub>2</sub> separation process.<sup>3</sup> The benefits of membrane-based separation technology, including its low cost, ease of preparation, and high separation efficiency,<sup>4-6</sup> have drawn the attention of researchers in addition to more conventional separation techniques like cryogenic distillation,<sup>7</sup> pressure swing adsorption (PSA),<sup>7</sup> and chemical adsorption.<sup>8</sup> Theoretically, membrane-based separation based on the dissolution-diffusion mechanism or size sieving is feasible because H<sub>2</sub> and CO<sub>2</sub> have similar dynamic diameters (H<sub>2</sub>: 2.9 Å, CO<sub>2</sub>: 3.3 Å),<sup>9</sup> but they differ greatly in polarity (CO<sub>2</sub> is a polar molecule, and H<sub>2</sub> is a non-polar molecule).<sup>10</sup> Although inorganic membranes have excellent thermal stability, their brittleness and high manufacturing cost limit large-scale application.<sup>11</sup> Polymeric membranes are susceptible to the trade-off effect,<sup>12</sup> which results in decreased selectivity. Consequently, a focal point of study in this domain is the development of innovative membrane materials characterized by elevated permeance, superior selectivity, and operational durability.

Metal-organic frameworks (MOFs) can be categorized as a type of crystalline porous materials that possess periodic network configurations, tunable pore size, functional structure and excellent specific surface area have been widely used in gas storage and separation,<sup>13, 14</sup> catalysis,<sup>15</sup> sensing<sup>16</sup> et al. Zeolitic imidazolate frameworks (ZIFs), a category of metal-organic frameworks (MOFs), have garnered significant interest owing to their structural similarity and superior stability compared to

<sup>a</sup> School of Chemistry and Chemical Engineering, Yangzhou University, Yangzhou, 225009, China

<sup>b</sup> Key Laboratory of Green and High-end Utilization of Salt Lake Resources, Qinghai Engineering and Technology Research Center of Comprehensive Utilization of Salt Lake Resources, Qinghai Institute of Salt Lakes, Chinese Academy of Sciences, Xining 810008, China

<sup>†</sup> These authors are equal to this work

<sup>\*</sup> Corresponding author

Electronic Supplementary Information (ESI) available: [details of any supplementary information available should be included here]. See DOI: 10.1039/x0xx00000x



inorganic zeolite materials.<sup>17</sup> ZIFs are self-assembled by transition metal ions (such as  $\text{Zn}^{2+}$ ,  $\text{Co}^{2+}$ ) and imidazole ligands. Their topological structure is similar to that of traditional zeolites, but they have more flexible pore size control capabilities and excellent chemical stability.<sup>18</sup> The crystal structure of ZIF-L is different from the cubic topology of traditional three-dimensional zeolites but is stacked in a two-dimensional layered form.<sup>19</sup> Its basic structural unit is a tetrahedral structure formed by the coordination of metal ions ( $\text{Zn}^{2+}$  or  $\text{Co}^{2+}$ ) with four imidazole ligands, but these tetrahedrons form a layered network by sharing ligands. ZIF-L has two pore structures: interlayer confined channels formed by stacking between adjacent layers and six-membered ring windows formed by imidazole rings within the layers. The pore size of the interlayer confined channels is about 0.3 nm, which is close to the molecular size of  $\text{H}_2$  and  $\text{CO}_2$ , and is suitable for separation based on molecular sieving effects. The pore size of the six-membered ring window formed by imidazole rings within the layer is about 0.4 nm, which can be used as a channel for rapid gas diffusion.<sup>20</sup> However, single metal ZIF-L membranes continue to have issues such as high pore stiffness and a single chemical environment, limiting further progress in separation performance. To overcome the performance bottleneck of single-metal ZIF materials, researchers have advocated synergistically optimizing the membrane's pore size, surface chemistry, and mechanical properties by the use of heterostructures ZIF systems.<sup>21</sup>

The most frequent approach for creating heterostructures is heteroepitaxial growth.<sup>22</sup> Heteroepitaxial development is a useful approach for designing the properties of crystalline materials by integrating distinct crystal systems *via* molecular-level interactions. Unlike other MOF modification strategies (such as metal/ligand exchange and covalent/click chemistry on ligand side chain groups), this method of connecting two different crystal systems at the molecular level can produce mixed crystals with combined properties while preserving the intrinsic properties of individual crystals.<sup>23</sup> This distinct advantage of heteroepitaxial growth allows us to generate a sequence of multi-level MOF structures that cannot be obtained by other means.<sup>24, 25</sup> It is worth noting that some zeolite films and membranes are made using heteroepitaxial growth methods.<sup>26, 27</sup> Co-ZIF-L replaces the  $\text{Zn}^{2+}$  in ZIF-L with  $\text{Co}^{2+}$ , but the crystal structure remains same. Furthermore, cobalt ions have a better coordination effect with dimethylimidazole, which can significantly improve the  $\text{H}_2/\text{CO}_2$  separation performance of ZIF-L.<sup>28, 29</sup>

The formation of crystals may be successfully controlled and the binding force between the MOF membrane and the support improved by network cross-linking chelated metal ions to aid in the diffusion growth of the interface.<sup>30</sup> In this work, polyvinyl alcohol (PVA) and polyallylamine (PAH) were used to cross-link chelated zinc ions, and the ZIF-L seed layer was constructed by diffusion growth at the interface, followed by secondary growth to fabricate a homogeneous heterostructure Co-Zn-ZIF-L membrane with high permeance and  $\text{H}_2/\text{CO}_2$  separation selectivity. The arrangement and orientation of the ZIF-L membrane were altered by optimizing the polymer layer and regulating the growth orientation, and the effects of various circumstances on  $\text{H}_2/\text{CO}_2$  selectivity and surface morphology were evaluated (Fig. 1).

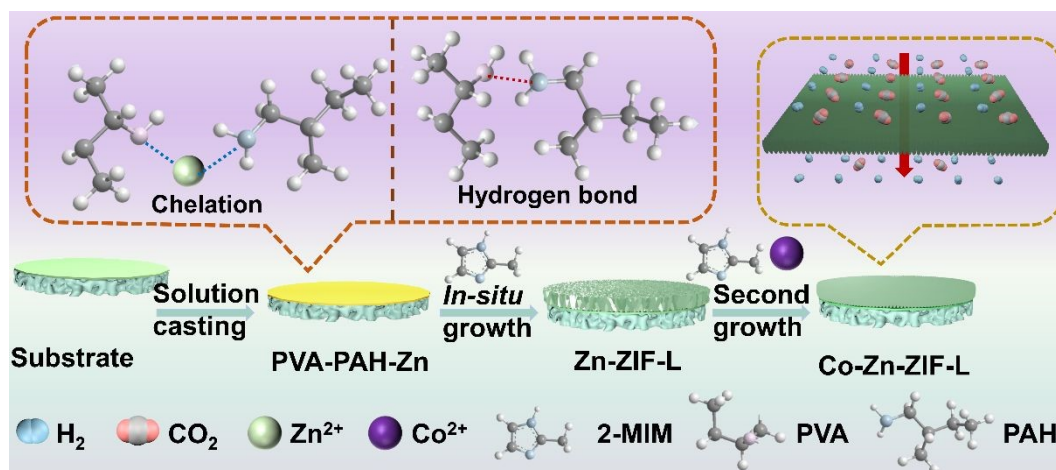


Fig. 1 Schematic of the preparation of the Co-Zn-ZIF-L membrane.

## 2. Results and discussion

The poor contact between ZIF-L and the PSf support makes it challenging to develop ZIF-L membranes directly on PSf support. The ZIF-L seeding layer was constructed by interfacial diffusion assisted by PVA-PAH chelated  $\text{Zn}^{2+}$ , and a continuous, defect-free homogeneous heterostructure Co-Zn-ZIF-L membrane was prepared by secondary growth on the Zn-ZIF-L surface by using an epitaxial growth strategy. The PVA and PAH network cross-linking was used to chelate  $\text{Zn}^{2+}$  to prepare a smooth surface with low roughness the PVA-PAH-Zn membrane (Fig. S2 and S3). The ZIF-L membrane prepared by *in-situ* growth does not show selective absence of peaks and showed no obvious orientation growth (Fig. S4 and S5). The polymer network's adhesion and cross-linking capabilities limit metal ion and ligand diffusion, allowing ZIF-L nanosheets to form orderly at the interface. The cross-linked polymer covers surface imperfections in the support, producing homogeneous nucleation sites for



secondary growth. The polymer's active groups ( $-\text{NH}_2$ ,  $-\text{OH}$ ) establish hydrogen or coordination bonds with the support and ZIF-L, which improves membrane adherence. The polymer network creates a dense and aligned ZIF-L seed layer with a (100) crystal plane parallel to the carrier surface. This exposes lateral two-dimensional pores and creates an initial sieving path for  $\text{H}_2/\text{CO}_2$ . The thickness of the resulting Zn-ZIF-L membrane was approximately  $1\ \mu\text{m}$  and the surface roughness of the Zn-ZIF-L membrane increased (Fig. S4 and S6). The homogeneous heterostructure Co-Zn-ZIF-L membrane with obvious preferential orientation was prepared by epitaxial diffusion secondary growth and the thickness of the resulting membrane is approximately  $1.7\ \mu\text{m}$  (Fig. 2a, 2b and S7). Secondary growth fills the intercrystalline defects in the initial layer, resulting in a continuous, defect-free membrane structure. Co-introduction enhances the pore electron distribution of the Zn-ZIF-L, boosting the preferential adsorption and diffusion of  $\text{H}_2$  while also achieving molecular sieving through the pore size. The XRD results of the Co-Zn-ZIF-L membrane showed a relatively strong peak at  $2\theta$  of  $29.55^\circ$  and a relatively weak peak at  $2\theta$  of  $14.10^\circ$ . These peaks correspond to the (800) and (400) crystal planes, respectively. The significantly higher intensity of the (800) crystal plane indicated the preferential a-axis orientation of the Co-Zn-ZIF-L membrane (Fig. 2c). By comparing the XRD patterns of the PAH-assisted membranes prepared *via in-suit* growth and secondary growth, it can be observed that the PAH-Co-Zn-ZIF-L membrane expanded along the (112) and (800) crystal planes (Fig. S13). It can be considered as that the seed layer has an inductive influence on the secondary growth, allowing crystals to develop in the orientation direction.<sup>31</sup> The Co-Zn-ZIF-L is synthesized *via* epitaxial diffusion growth on the surface of a Zn-ZIF-L membrane, but Co-Zn-ZIF-L has preferred orientation growth and the membrane surface is not continuously formed, resulting in a higher surface roughness than the Zn-ZIF-L membrane (Fig. 2d). The cross-sectional EDS results of the Co-Zn-ZIF-L membrane show that Zn accounting for 7.13% is mainly in the lower half of the membrane layer and Co accounting for 20.07% is mainly in the upper half of the membrane layer, indicating that a homogeneous heterogeneous structure Co-Zn-ZIF-L membrane has been successfully constructed (Fig. 2e, S14 and S15).

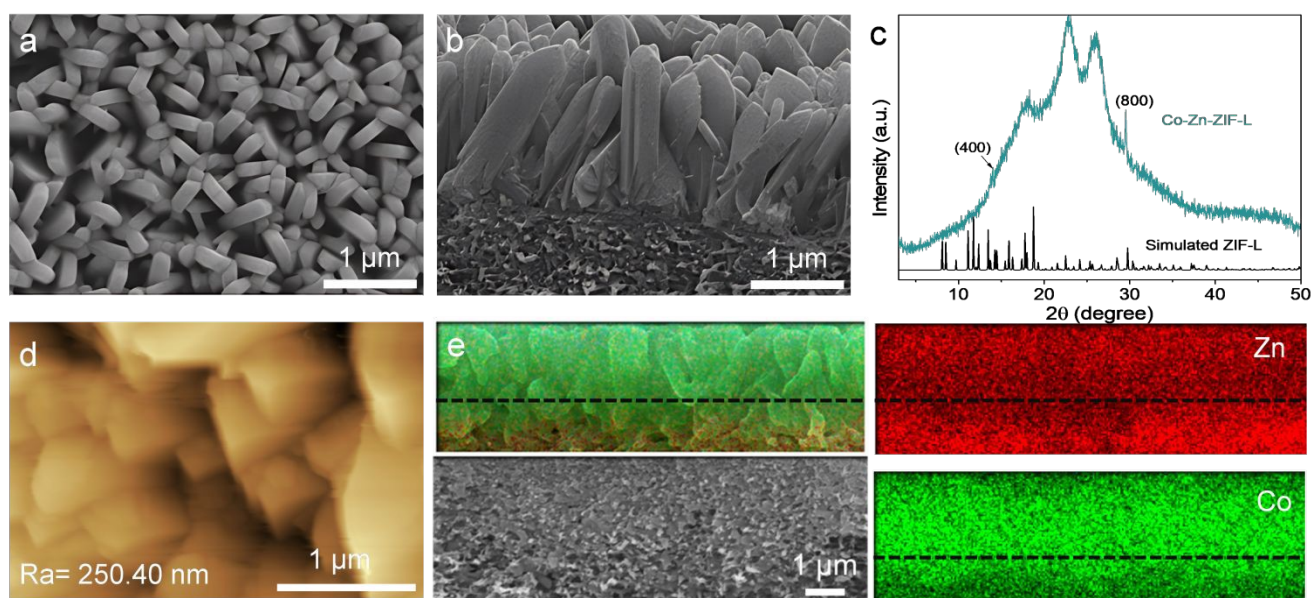


Fig. 2 Surface (a) and cross-sectional (b) SEM image of Co-Zn-ZIF-L membrane. (c) The simulated and experimental XRD patterns of Co-Zn-ZIF-L membrane. (d) The AFM image of Co-Zn-ZIF-L membrane. (e) The EDS image of the Co-Zn-ZIF-L membrane.

To investigate the influence of network cross-linked chelated metal-assisted interface diffusion on the membrane structure during the manufacture of ZIF-L membrane, total reflection Fourier transform infrared spectroscopy (ATR-FTIR) was used. The ATR-FTIR spectra of the PVA/PAH-Zn membrane revealed no discernible peak near  $400\ \text{cm}^{-1}$ , indicating that no clear coordination structure had formed at this point. However, the ATR-FTIR spectrum of the Zn-ZIF-L membrane revealed an evident but weak signal near  $400\ \text{cm}^{-1}$ , showing that the Zn-N coordination bond was formed initially. Following the second growth, the membrane thickness and peak intensity rose dramatically, indicating the development of Co-N and a more ordered ZIF-L structure (Fig. 3b). The ATR-FTIR spectra of resulting powders showed a similar peak augmentation pattern (Fig. 3a). We also performed ATR-FTIR analysis on PVA and PAH membranes, and the Zn-N/Co-N coordination peaks in the membranes followed the expected trend (Fig. S16 and S17). The ATR-FTIR spectra of the PVA/PAH-Zn membrane showed the characteristic peaks of both  $-\text{OH}$  and  $-\text{NH}_2$ , which further reflected the influence of network cross-linked chelated metal-assisted interface diffusion on the membrane structure during the manufacture of ZIF-L membrane. The adsorption of  $\text{H}_2$  and  $\text{CO}_2$  on Co-Zn-ZIF-L powders at 303 K reveals that Co-Zn-ZIF-L with a linear adsorption for  $\text{H}_2$  and a conventional Langmuir adsorption for  $\text{CO}_2$  (Fig. 3c and 3d). The  $\text{H}_2$  molecule is small and can freely enter the microporous structure of Co-Zn-ZIF-L. The interaction with Co-Zn-ZIF-L is modest, resulting in linear adsorption. The  $\text{CO}_2$  molecules are bigger and have a quadrupole moment. It can form a monolayer chemical adsorption with open metal sites (e.g.  $\text{Co}^{2+}$ ) or nitrogen-containing ligands in Co-



Zn-ZIF-L by dipole-quadrupole or acid-base interactions, exhibiting typical Langmuir adsorption behaviour. This differential in adsorption gives Co-Zn-ZIF-L a high potential for H<sub>2</sub>/CO<sub>2</sub> separation.

DOI: 10.1039/D5IM00114E

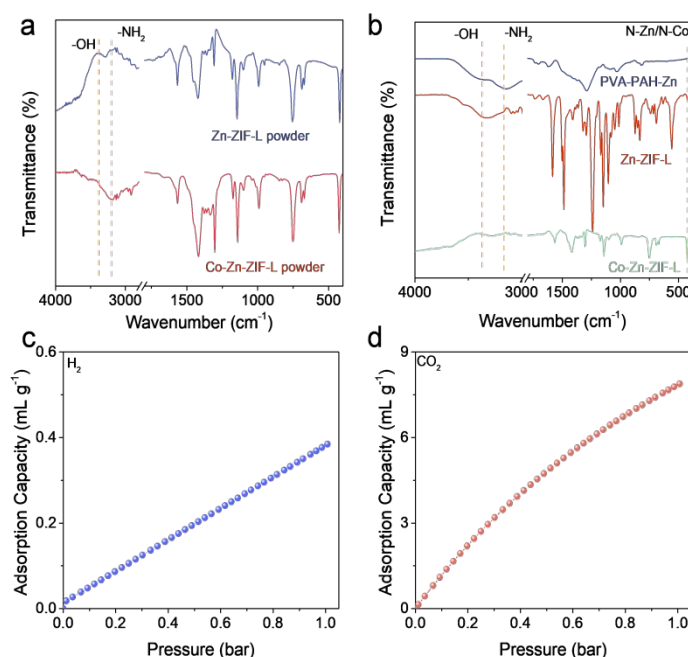


**Fig. 3** (a) ATR-FTIR spectrum of Zn-ZIF-L and Co-Zn-ZIF-L powders; (b) ATR-FTIR spectrum of PVA-PAH-Zn, Zn-ZIF-L and Co-Zn-ZIF-L membranes; The adsorption isotherms of Co-Zn-ZIF-L powder for H<sub>2</sub> (c) and CO<sub>2</sub> (d) at 303K.

To acquire a better knowledge of the intercrystalline structure of the secondary generated Co-Zn-ZIF-L membrane, the prepared Co-Zn-ZIF-L membrane's H<sub>2</sub>/CO<sub>2</sub> separation performance was evaluated by a Wicke-Kallenbach approach. The Co-Zn-ZIF-L membrane outperformed the PVA-Co-Zn-ZIF-L and PAH-Co-Zn-ZIF-L membranes in terms of H<sub>2</sub>/CO<sub>2</sub> separation performance, with an H<sub>2</sub> permeance of 2156 GPU and an H<sub>2</sub>/CO<sub>2</sub> selectivity of 31.6 (Fig. 4a). The separation performance of the constructed ZIF-L membrane surpassed the Robeson upper bound (2008), and when compared to H<sub>2</sub>/CO<sub>2</sub> separation membranes described in the literature, the ZIF-L membrane shown potential advantages (Fig. 4c). The solubility coefficient and diffusion coefficient of H<sub>2</sub> and CO<sub>2</sub> in the Co-Zn-ZIF-L membrane were calculated to analyse the transport mechanism of H<sub>2</sub> and CO<sub>2</sub> in the Co-Zn-ZIF-L membrane (Fig. 4b). The adsorption of CO<sub>2</sub> by the ZIF-L framework is substantially higher than that of H<sub>2</sub>, hence the CO<sub>2</sub> solubility coefficient of the Co-Zn-ZIF-L membrane is higher than that of H<sub>2</sub>. The diffusion differential of H<sub>2</sub>/CO<sub>2</sub> in the Co-Zn-ZIF-L membrane is the primary mechanism for H<sub>2</sub>/CO<sub>2</sub> separation. Considering the analysis of the source of performance, we tested the separation performance of PVA/PAH-Zn, Zn-ZIF-L, and Co-Zn-ZIF-L membranes. The results demonstrated that the high separation performance of Co-Zn-ZIF-L membrane stemmed from the ZIF-L structure with a porosity between that of H<sub>2</sub> and CO<sub>2</sub>. Furthermore, directed development of ZIF-L along the a-axis is essential for successful H<sub>2</sub>/CO<sub>2</sub> separation (Fig. 4d).<sup>32</sup>



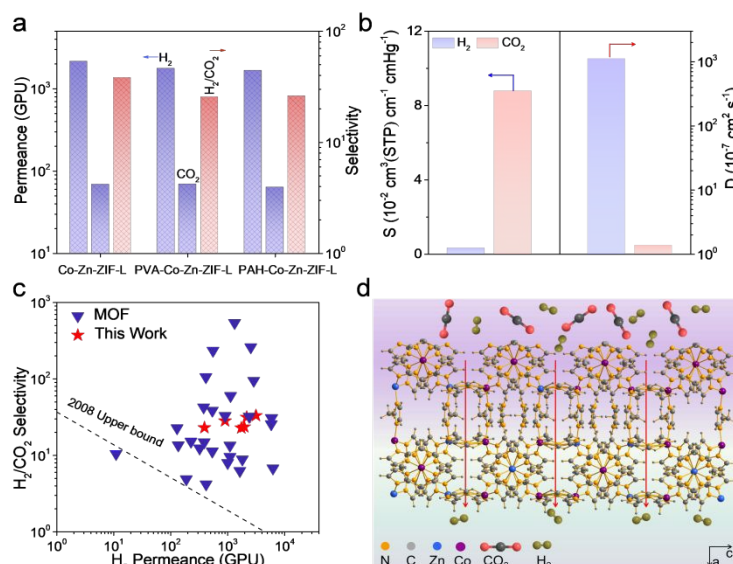


**Fig. 4** (a) Gas permeance and H<sub>2</sub>/CO<sub>2</sub> selectivity of resultant ZIF-L membranes. Feed pressure, 1.0 bar, temperature, 298 K, H<sub>2</sub> : CO<sub>2</sub>, 1:1; (b) Solubility coefficient and diffusion coefficient of Co-Zn-ZIF-L membrane for H<sub>2</sub> and CO<sub>2</sub> (the Co-Zn-ZIF-L membrane thickness is 1.7  $\mu$ m based on the cross-section SEM); (c) The performance comparison ZIF-L membranes in this work, Robeson upper bound, and the ZIF-L membranes reported in previous literatures (permeability was converted to a membrane thickness of 1  $\mu$ m for the permeance); (d) Schematic of the H<sub>2</sub> and CO<sub>2</sub> molecules permeate Co-Zn-ZIF-L framework along the a-axis.

The effect of feed temperature on the performance of Co-Zn-ZIF-L membrane was evaluated (Fig. 5a). The permeance of tested H<sub>2</sub> and CO<sub>2</sub> increased as temperature improved, indicating that there is activated diffusion of gas molecules in the Co-Zn-ZIF-L framework. The changes in separation performance of the Co-Zn-ZIF-L membrane were studied under various pressure conditions. The permeance of H<sub>2</sub> and CO<sub>2</sub> reduced as pressure climbed (Fig. 5b). It is possible that Co-Zn-ZIF-L has a better adsorption capacity for CO<sub>2</sub>. As the pressure rises, the amount of CO<sub>2</sub> adsorbed in the ZIF-L pores increases dramatically, occupying more diffusion sites and blocking H<sub>2</sub> permeation. The CO<sub>2</sub> permeance decreases due to adsorption saturation, but H<sub>2</sub> diffusion is significantly impeded, resulting in a loss of selectivity. The H<sub>2</sub> purification requires a high level of membrane stability. In this investigation, the membrane's separation ability under dry and wet circumstances was assessed (Fig. 5c). During 65 hours of continuous evaluation in dry conditions, the membrane maintained a nearly constant H<sub>2</sub> permeance (approximately 2100 GPU) and H<sub>2</sub>/CO<sub>2</sub> selectivity (around 32). The addition of water vapor to the feed reduced the permeance of H<sub>2</sub> and CO<sub>2</sub>. The water transport segment of the membrane used the H<sub>2</sub> and CO<sub>2</sub> channels. This blocking effect is more noticeable for larger CO<sub>2</sub> molecules, which increases the H<sub>2</sub>/CO<sub>2</sub> selectivity. To verify the results, we performed molecular dynamics simulation (MSD) and diffusion coefficient tests on Co-Zn-ZIF-L powder. The study found that the diffusion coefficient of H<sub>2</sub> was significantly higher than that of CO<sub>2</sub>, indicating that CO<sub>2</sub> encountered greater resistance when permeating the membrane layer (Fig. 5d, 5e and 5f). The Zn-ZIF-L membrane exhibited high flux but poor selectivity, which further confirmed the impact of the synergistic effect between Zn and Co bimetals on the membrane performance.



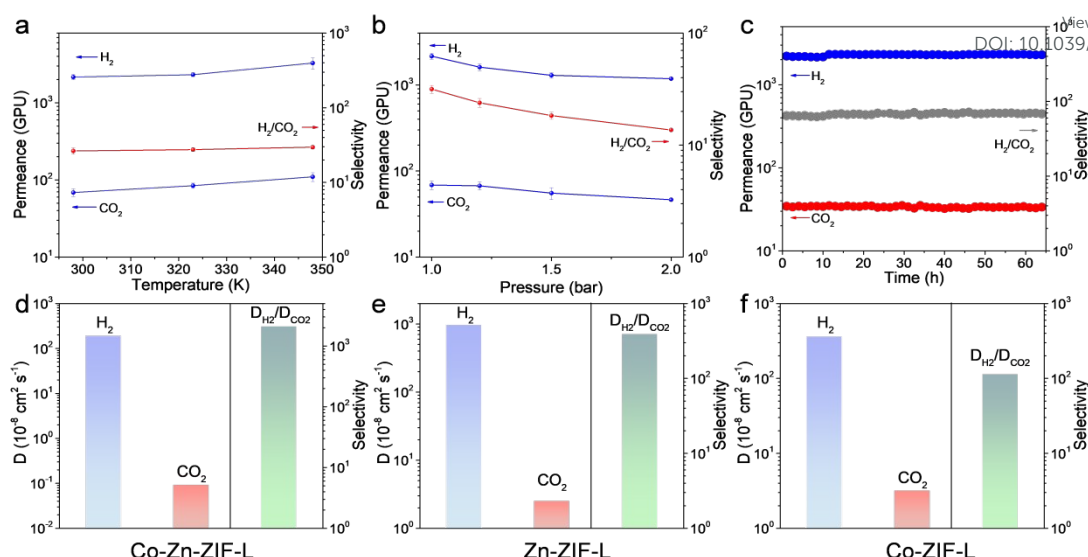


Fig. 5 The H<sub>2</sub>/CO<sub>2</sub> separation performance of Co-Zn-ZIF-L membrane at different operation temperature (a) and pressure (b); (c) Operational stability of the Co-Zn-ZIF-L membrane for H<sub>2</sub>/CO<sub>2</sub> separation. Feed pressure, 1.0 bar, temperature, 298 K, H<sub>2</sub> : CO<sub>2</sub>, 1:1; The diffusion coefficient of (d) Co-Zn-ZIF-L, (e) Zn-ZIF-L and (f) Co-ZIF-L for H<sub>2</sub> and CO<sub>2</sub> calculated by molecular dynamics simulation.

### 3. Conclusions

To achieve efficient H<sub>2</sub>/CO<sub>2</sub> separation, the orientation growth of ZIF-L was regulated by polymer cross-linking coupling-assisted interfacial diffusion. A continuous, defect-free a-axis-oriented heterostructure Co-Zn-ZIF-L membrane was built on the surface of a porous substrate. This strategy effectively controlled the directional assembly and tight stacking of ZIF-L nanosheets at the interface by introducing a polymer cross-linking network, significantly inhibited the formation of non-selective defects, and improved the membrane layer's mechanical stability and interfacial bonding strength. The synthesized Co-Zn-ZIF-L membrane demonstrated superior H<sub>2</sub>/CO<sub>2</sub> separation performance. The H<sub>2</sub> permeance reached 2156 GPU, while the H<sub>2</sub>/CO<sub>2</sub> selectivity was as high as 31.6 at 298 K and 1.0 bar, far surpassing the Robeson upper bound (2008) and outperforming most reported ZIF-based separation membranes. Mechanistic studies have revealed that the synergistic action of Co and Zn improves the microenvironment of ZIF-L pores. The polymer cross-linking coupling-assisted interface diffusion control strategy creates an oriented growth dense membrane structure. This allows for rapid screening and transmission of H<sub>2</sub> molecules in sub-nanometer pores while effectively blocking CO<sub>2</sub> molecules through pore confinement and surface diffusion. This work not only gives new ideas for the green preparation of high-performance MOF membranes, but it also provides critical material support for boosting the development of efficient gas separation technology in the context of hydrogen economy and carbon neutrality.

### 4. Experimental section

#### Materials

Polyvinyl alcohol (PVA, Mw = 2-200 kDa, 99%), Co(NO<sub>3</sub>)<sub>2</sub>·6H<sub>2</sub>O (99%), and 2-methylimidazole (C<sub>4</sub>H<sub>6</sub>N<sub>2</sub>, 99%) were purchased from Aladdin Reagents (Shanghai) Co., Ltd.. Polyacryl Ammonium hydrochloride (PAH, Mw = 10-20 kDa) was obtained from Beijing Huawei Ruiké Chemical Co., Ltd.. Zn(NO<sub>3</sub>)<sub>2</sub>·6H<sub>2</sub>O (99%) was purchased from Sinopharm Reagent Co., Ltd.. Anhydrous ethanol was purchased from Hongbaoli (Beijing) Co., Ltd.. Deionized water is made in the laboratory. All reagents were used without further purification.

#### The preparation of Co-Zn-ZIF-L membranes

**Fabrication of Zn-ZIF-L membranes:** To make a 4% PVA solution, the PVA was mixed with water and refluxed and agitated for 12 hours at 80 °C. The PAH was added to water and agitated at room temperature for 30 minutes to produce a 4% PAH solution. Take an equal amount of the PVA solution and PAH solution, mix them together to obtain the 2 wt% PVA/PAH solution. The 2.97 g Zn(NO<sub>3</sub>)<sub>2</sub>·6H<sub>2</sub>O was added to 100 mL the PVA/PAH solution, PVA solution and PAH solution to prepare the PVA/PAH-Zn<sup>2+</sup>, PVA-Zn<sup>2+</sup> and PAH-Zn<sup>2+</sup> solution. The PVA/PAH-Zn<sup>2+</sup> membrane layer was then prepared by applying a certain amount of PVA/PAH-Zn<sup>2+</sup> solution to the Psf support and drying it at 50 °C for 12 h. Subsequently, The ZIF-L membrane was prepared by adding 2-MIM at a concentration of 0.8 mol L<sup>-1</sup> and react for 2 h and washed with anhydrous ethanol several times. The PVA-ZIF-L and PAH-ZIF-L membranes were prepared using the same method.



Preparation of Co-Zn-ZIF-L membranes: The Co-Zn-ZIF-L membrane was fabricated by secondary growth, as follows: 1 mL of  $\text{Co}(\text{NO}_3)_2 \cdot 6\text{H}_2\text{O}$  solution ( $0.1 \text{ mol L}^{-1}$ ) and 2 mL of 2-MIM solution ( $0.8 \text{ mol L}^{-1}$ ) were added to the previously made ZIF-L membrane and react for 4 hours, followed by washing with sewage ethanol and drying to obtain a homogeneous heterogeneous Co-Zn-ZIF-L membrane. The PVA-Co-Zn-ZIF-L and PAH-Co-Zn-ZIF-L membranes were prepared using the same process.

#### Preparation of MOF powders

All MOF powders were extracted from the corresponding mother solutions after the fabrication of membranes and were washed with ethanol by centrifugation and dried for further use.

#### Characterizations

The morphology of samples was observed by scanning electron microscope (SEM, Zeiss\_Supra55) under the acceleration voltage of 5.0 kV. EDS mapping images were captured on a Gemini 300 transmission electron microscope. The material's crystal structure was studied using X-ray diffraction (XRD) on a Bruker D8 Advanced X-ray Diffractometer ( $\text{Cu-K}\alpha$  radiation:  $\lambda = 0.154 \text{ nm}$ ). The ATR-FTIR spectrum of samples was recorded in the range of 500 to  $4000 \text{ cm}^{-1}$  on a Cary 610/670 Microscopic Infrared Spectrometer IR (Cary 610/670). The AFM images were obtained from SPM-9700HT Atomic Force Microscope. The gas adsorption isotherms of ZIF-L powders were measured using the pressure decay method. The  $\text{H}_2$  and  $\text{CO}_2$  adsorption of ZIF-L powders was evaluated by BSD-PM (PM2-1516-B) analyser at 303 K. The ZIF-L particles were activated at  $120^\circ\text{C}$  for 24 h before the adsorption test.

#### Gas permeation experiments

The gas separation performance test was carried out at room temperature. With  $\text{H}_2$  and  $\text{CO}_2$  having a feed flow rate of  $30 \text{ mL min}^{-1}$  respectively, argon (99.99%) acts as the sweep gas, with its flow rate of  $20 \text{ mL min}^{-1}$ . All the gases were purchased from Jiulong Company of Yangzhou. For the performance test, detection was performed using a Fuli F70 gas chromatograph equipped with a highly sensitive thermal conductivity detector (TCD). The test process device is shown in Fig S1.

Equation (1) was employed to determine the gas permeance:

$$P_i = \frac{N_i}{\Delta p_i \cdot A} \quad (1)$$

within this equation (1),  $P_i$  (measured in  $\text{mol m}^{-2} \text{ s}^{-1} \text{ Pa}^{-1}$ ),  $N_i$  (in  $\text{mol s}^{-1}$ ) and  $\Delta P$  (Pa) represent the gas permeance of component i, its molar flow under standard state conditions, and the transmembrane pressure drop, respectively. The symbol  $S$  ( $\text{m}^2$ ) designates the effective area of the membrane. For ease of comparison, gas permeance values are commonly converted to GPU units, with 1 GPU equivalent to  $3.348 \times 10^{-10} \text{ mol m}^{-2} \text{ s}^{-1} \text{ Pa}^{-1}$ .

Equation (2) was employed to determine the gas permeance:

$$\alpha_{\text{H}_2/\text{CO}_2} = \frac{P_{\text{H}_2}}{P_{\text{CO}_2}} \quad (2)$$

within this equation (2),  $P_i$  and  $P_j$  represent the gas permeance coefficients of component i and component j, calculated under identical experimental conditions, respectively.

#### Author Contributions

S. C. and S. S. conceived the idea, designed the experiments, measured the  $\text{H}_2/\text{CO}_2$  separation performance, interpreted the data, and wrote the paper. S. S. prepared membranes. Y. Z. and M. W. analysed the morphology of ZIF-L membranes. Z. J. and Y. Z. analysed the data. J. P. secured the funding and provided EDS line-scan test. H. P. supervised and secured the funding. All authors contributed to reviewing, editing, and revising the paper.

#### Conflicts of interest

The authors declare no conflict of interest.

#### Acknowledgements

This work was financially supported by the Project for International Cooperation in Science and Technology, Qinghai Province (No. 2024- HZ-804), Yangzhou "Green Yang Jinfeng Plan" excellent doctor talent funding program and Yangzhou University Startup Fund for Distinguished Scholars (137013525).

#### References

1. L. M. Germeshuizen and P. W. E. Blom, A techno-economic evaluation of the use of hydrogen in a steel production process, utilizing nuclear process heat, *Int. J. Hydrog. Energy*, 2013, **38**, 10671-10682.
2. S. P. Cardoso, A. I. S., L. Zhi, P. Inês, R. A. E. and C. M. and Silva, Inorganic membranes for hydrogen separation, *Sep. Purif. Rev.*, 2018, **47**, 229-266.





3. C. Y. Chuah, J. Lee and T.-H. Bae, Graphene-based membranes for H<sub>2</sub> separation: Recent progress and future perspective, *Membranes*, 2020, **10**, 336.
4. J. Wang, C. Yuan, C. Li, G. Geng, J. Song, N. Yang, S. Kawi, J. Sunarso, X. Tan and S. Liu, Nickel-based metallic membranes for hydrogen production in membrane reactor: A brief overview, *Sep. Purif. Technol.*, 2024, **358**, 130435.
5. J. Fu, S. Das, G. Xing, T. Ben, V. Valtchev and S. Qiu, Fabrication of COF-MOF composite membranes and their highly selective separation of H<sub>2</sub>/CO<sub>2</sub>, *J. Am. Chem. Soc.*, 2016, **138**, 7673-7680.
6. M. Liu, J. Emery and R. Guo, Microporous pentiptycene-based polybenzimidazole membranes for high temperature H<sub>2</sub>/CO<sub>2</sub> separation, *J. Membr. Sci.*, 2025, **718**, 123673.
7. Y. Ko, J.-H. Kang, H. Do, J. Kum and C.-H. Lee, Hybrid process using cryogenic and pressure swing adsorption process for CO<sub>2</sub> capture and extra H<sub>2</sub> production from a tail gas in a steam methane reforming plant, *Energy Convers. Manag.*, 2025, **328**, 119561.
8. L. F. A. S. Zafaneli, E. Aly, A. E. Rodrigues and J. A. C. Silva, A novel cryogenic fixed-bed adsorption apparatus for studying green hydrogen recovery from natural gas grids, *Sep. Purif. Technol.*, 2023, **307**, 122824.
9. Y. Peng, Y. Li, Y. Ban, H. Jin, W. Jiao, X. Liu and W. Yang, Metal-organic framework nanosheets as building blocks for molecular sieving membranes, *Science*, 2014, **346**, 1356-1359.
10. H. Li, L. Han, J. Hou, J. Liu and Y. Zhang, Oriented zeolitic imidazolate framework membranes within polymeric matrices for effective N<sub>2</sub>/CO<sub>2</sub> separation, *J. Membr. Sci.*, 2019, **572**, 82-91.
11. M. S. Denny, J. C. Moreton, L. Benz and S. M. Cohen, Metal-organic frameworks for membrane-based separations, *Nat. Rev. Mater.*, 2016, **1**, 16078.
12. H. B. Park, J. Kamcev, L. M. Robeson, M. Elimelech and B. D. Freeman, Maximizing the right stuff: The trade-off between membrane permeability and selectivity, *Science*, 2017, **356**, eaab0530.
13. A. Felix Sahayaraj, H. Joy Prabu, J. Maniraj, M. Kannan, M. Bharathi, P. Diwahar and J. Salamon, Metal-organic frameworks (MOFs): The next generation of materials for catalysis, gas storage, and separation, *J. Inorg. Organomet. Polym. Mater.*, 2023, **33**, 1757-1781.
14. S. K. B., K. Aswini, A. K. Rao, K. Alam, M. S. Mashkour and A. Jain, Fabrication and characterization of nanoscale metal-organic frameworks (MOFs) for gas storage and separation, *E3S Web Conf.*, 2023, **430**, 01124.
15. M. Martos and I. M. Pastor, Node modification of metal-organic frameworks for catalytic applications, *ChemistryOpen*, 2025, e202400428.
16. S. Zhang, M. Wang, X. Wang, J. Song and X. Yang, Electrocatalysis in MOF films for flexible electrochemical sensing: A comprehensive review, *Biosensors*, 2024, **14**, 420.
17. K. S. Park, Z. Ni, A. P. Côté, J. Y. Choi, R. Huang, F. J. Uribe-Romo, H. K. Chae, M. O'Keeffe and O. M. Yaghi, Exceptional chemical and thermal stability of zeolitic imidazolate frameworks, *Proc. Natl. Acad. Sci. U.S.A.*, 2006, **103**, 10186-10191.
18. G. Chen, G. Liu, Y. Pan, G. Liu, X. Gu, W. Jin and N. Xu, Zeolites and metal-organic frameworks for gas separation: The possibility of translating adsorbents into membranes, *Chem. Soc. Rev.*, 2023, **52**, 4586-4602.
19. F. Şahin, B. Topuz and H. Kalıpçılar, Synthesis of ZIF-7, ZIF-8, ZIF-67 and ZIF-L from recycled mother liquors, *Micropor. Mesopor. Mater.*, 2018, **261**, 259-267.
20. Z.-X. Low, J. Yao, Q. Liu, M. He, Z. Wang, A. K. Suresh, J. Bellare and H. Wang, Crystal transformation in zeolitic-imidazolate framework, *Cryst. Growth Des.*, 2014, **14**, 6589-6598.
21. J. K. Zaręba, M. Nyk and M. Samoć, Co/ZIF-8 heterometallic nanoparticles: Control of nanocrystal size and properties by a mixed-metal approach, *Cryst. Growth Des.*, 2016, **16**, 6419-6425.
22. H. T. Kwon, H.-K. Jeong, A. S. Lee, H. S. An and J. S. Lee, Heteroepitaxially grown zeolitic imidazolate framework membranes with unprecedented propylene/propane separation performances, *J. Am. Chem. Soc.*, 2015, **137**, 12304-12311.
23. A. D. Burrows, Mixed-component metal-organic frameworks (MC-MOFs): Enhancing functionality through solid solution formation and surface modifications, *CrystEngComm*, 2011, **13**, 3623-3642.
24. S. Furukawa, K. Hirai, Y. Takashima, K. Nakagawa, M. Kondo, T. Tsuruoka, O. Sakata and S. Kitagawa, A block PCP crystal: Anisotropic hybridization of porous coordination polymers by face-selective epitaxial growth, *Chem. Commun.*, 2009, 5097-5099.
25. T. T. Y. Tan, J. T. M. Cham, M. R. Reithofer, T. S. Andy Hor and J. M. Chin, Motorized Janus metal organic framework crystals, *Chem. Commun.*, 2014, **50**, 15175-15178.
26. S. Y. Toru Wakihara, Kumiko Iezumi, and Tatsuya Okubo, Heteroepitaxial growth of a zeolite film with a patterned surface-texture, *J. Am. Chem. Soc.*, 2003, **125**, 12388-12389.
27. H.-K. Jeong, J. Krohn, K. Sujaoti and M. Tsapatsis, Oriented molecular sieve membranes by heteroepitaxial growth, *J. Am. Chem. Soc.*, 2002, **124**, 12966-12968.
28. X. Zeng, W. Zhou, P. Zhou, M. Zhang, C. Zhou, L. Tan and L. Wang, ZIF-L(Co) coated stainless steel meshes with superwettability for efficient multiphase liquid separation, *J. Environ. Chem. Eng.*, 2021, **9**, 105325.
29. S. Mo, Q. Zhang, Q. Ren, J. Xiong, M. Zhang, Z. Feng, D. Yan, M. Fu, J. Wu, L. Chen and D. Ye, Leaf-like Co-ZIF-L derivatives embedded on Co<sub>2</sub>AlO<sub>4</sub>/Ni foam from hydrotalcites as monolithic catalysts for toluene abatement, *J. Hazard. Mater.*, 2019, **364**, 571-580.
30. L. Yang, Z. Wang and J. Zhang, Highly permeable zeolite imidazolate framework composite membranes fabricated via a chelation-assisted interfacial reaction, *J. Mater. Chem. A*, 2017, **5**, 15342-15355.
31. J. Yan, T. Ji, Y. Sun, S. Meng, C. Wang and Y. Liu, Room temperature fabrication of oriented Zr-MOF membrane with superior gas selectivity with zirconium-oxo cluster source, *J. Membr. Sci.*, 2022, **661**, 120959.
32. K. Yang, S. Hu, Y. Ban, Y. Zhou, N. Cao, M. Zhao, Y. Xiao, W. Li and W. Yang, ZIF-L membrane with a membrane-interlocked-support composite architecture for H<sub>2</sub>/CO<sub>2</sub> separation, *Sci. Bull.*, 2021, **66**, 1869-1876.



# Design and construction of homogeneous heterogeneity Co-Zn-ZIF-L membranes for efficient H<sub>2</sub>/CO<sub>2</sub> separation

Shenzhen Cong,<sup>†a</sup> Si Sun,<sup>†a</sup> Yijing Zhang,<sup>a</sup> Ming Wang,<sup>a</sup> Zhehua Jia,<sup>a</sup> Jiaoyu Peng<sup>\*b</sup> and Huan Pang<sup>\*a</sup>

<sup>a</sup> School of Chemistry and Chemical Engineering, Yangzhou University, Yangzhou, 225009, China

<sup>b</sup> Key Laboratory of Green and High-end Utilization of Salt Lake Resources, Qinghai Engineering and Technology Research Center of Comprehensive Utilization of Salt Lake Resources, Qinghai Institute of Salt Lakes, Chinese Academy of Sciences, Xining 810008, China

<sup>†</sup> These authors are equal to this work

\* Corresponding author: panghuan@yzu.edu.cn, pengjy@isl.ac.cn

## Data availability statement:

The authors support the data underlying the results reported in this paper, and all data are presented in the main text and supporting information.

